JSST
Journal of Space Science and Technology

P-ISSN: 2008-4560
E-ISSN: 2423-4516

Journal of Space Science and Technology

Vol. 19, No. 3, pp. 81-91, 2026
https://doi.org/10.22034/jsst.2025.1574
Journal Homepage: https://jsstpub.com



Original Research Paper

Implementation of a Single-Degree-of-Freedom Rotary Inertial Navigation System Based on Low-Cost Inertial Sensors

Alireza Sharifi* and **Amir Eslami**

Department of Aerospace Engineering, Sharif University of Technology, Tehran, Iran

ARTICLE INFO

Article History:

Received 12 August 2025
Revised 29 October 2025
Accepted 22 November 2025
Available Online 02 December 2025

Keywords:

Rotary inertial navigation system
Error reduction
Error modeling
Experimental validation
Sensor errors

ABSTRACT

In conventional inertial navigation systems (INS), the error accumulation due to the integration process leads to drift in the actual values of position, velocity, and attitude of an unmanned aerial vehicle. In this study, to mitigate such accumulated errors, a rotating inertial navigation system (RINS) is implemented around the vertical axis using low-cost inertial measurement unit (IMU) sensors. First, the influence of various error sources—including bias, scale factor, and misalignment errors—over time in a static scenario is analyzed for the rotary configuration. Then, a comparative evaluation is performed against a conventional INS. Subsequently, the effect of each error source is investigated in a dynamic test through software simulation of a single-degree-of-freedom RINS, with results compared to those of the conventional INS simulation. Moreover, to validate the simulation results, experimental tests are designed and conducted to assess the accuracy of the rotary inertial navigation system under real-world conditions. Finally, the RINS is implemented on a single-degree-of-freedom rate table in the Control Systems Laboratory environment of the aerospace department of Sharif University. The results demonstrate that the RINS configuration effectively reduces bias, scale factor, and misalignment errors around the body's x and y axes.

* Corresponding Author's E-mail: ar.sharifi@sharif.edu

How to Cite this Article:
A. Sharifi and A. Eslami, "Implementation of a single-degree-of-freedom rotary inertial navigation system based on low-cost inertial sensors," *Journal of Space Science and Technology*, Vol. 19, No. 3, pp. 81-91, 2026, https://doi.org/10.22034/jsst.2025.1574.

COPYRIGHTS
© 2026 by the authors. Published by ARI. This article is an open access article distributed under the terms and conditions of The Creative Commons Attribution 4.0 International (CC BY 4.0)

NOMENCLATURE

L	Geographic latitude
λ	Geographic longitude
h	Body's altitude above the Earth's surface
$\dot{L}$	Rate of change of geographic latitude
$\dot{\lambda}$	Rate of change of geographic longitude
$\dot{h}$	Rate of change of altitude

Table of Acronyms

INS	Inertial Navigation System
SINS	Strapdown Inertial Navigation System
RINS	Rotating Inertial Navigation System
IMU	Inertial Measurement Unit
AHRS	Attitude and Heading Reference System

1. INTRODUCTION

With the advancement of navigation technologies, Inertial Navigation Systems (INS) [1] have become one of the most critical tools for determining position and guiding various types of vehicles, including aircraft, submarines, missiles, and spacecraft. Operating independently of external signals, these systems estimate position, velocity, and attitude by integrating the vehicle's measured acceleration and angular rate provided by the inertial measurement unit (IMU) [2]. Owing to their high autonomy, high sampling rate, and robustness against environmental conditions, INS are widely adopted in modern navigation applications.

INS can generally be classified into two main categories: stable platform INS [3] and strapdown INS (SINS) [4], depending on how the IMU is mounted. In stable platform systems, the IMU is mechanically isolated from the vehicle's rotations by mounting it on a gimbaled platform, whereas in SINS, the IMU is rigidly attached to the vehicle's body [5]. Owing to their lower cost, smaller size, and higher reliability, SINS configurations are widely adopted in modern navigation systems. However, they are more susceptible to initialization errors, sensor biases, and other types of measurement errors, which can lead to significant navigation inaccuracies over time.

One of the primary challenges in INS particularly in SINS is the cumulative error resulting from sensor bias and drift, which causes gradual degradation of navigation accuracy and may eventually lead to divergence. To enhance performance and mitigate these errors, various techniques have been developed, such as INS/GPS integration, Attitude and Heading Reference Systems (AHRS), transfer alignment [6], and the rotating inertial navigation system (RINS) [7]. In this study, the focus is placed on the Low-Cost Rotary Inertial Navigation System, which has proven effective in reducing several types of errors by continuously rotating the inertial sensors around a specific axis. This rotation helps to average out systematic biases, thereby decreasing overall navigation errors and improving system accuracy.

In 1968, Geller described a gimbaled inertial navigation system in which the platform continuously rotated relative to the local horizontal frame. He concluded that the system's position error could be significantly reduced by using rotation frequencies greater than twice the Schuler frequency [8]. In 1980, Levinson and Giovannini, and later in 1981, Giovannini and Levinson, implemented this technique on a strapdown inertial navigation system and proposed a marine navigation solution based on a ring laser gyroscope [9]. In 2004, Yang and Miao, in 2009, Zhang *et al.*, and in 2010, Ben *et al.*, analyzed the principle of error modulation through continuous rotation of the inertial measurement unit (IMU) around the vertical axis [10,11,7]. In 2015, Du Shuang, in his PhD Thesis, compared installation, bias, and scale factor errors in conventional and rotating inertial navigation systems using theoretical analyses and numerical simulations. Furthermore, the potential integration of the rotating inertial navigation system with the global positioning system (GPS) was also examined [12]. In 2017, Tianxiao Song et al. described a rotation scheme for rapid and precise initial alignment in DRINS. By introducing two design principles to enhance observability and employing a Kalman filter, the proposed method improves estimation accuracy. Simulation and experimental results confirm its effectiveness compared to traditional approaches [13].

In 2019, Zengjun Liu ET AL. Analyzed attitude accuracy loss in tri-axis rotational inertial navigation systems (RINS) caused by rotation mechanism errors. A recursive least squares (RLS)-based self-calibration method was proposed to compensate for these errors. Experiments showed that the technique greatly improved short-term attitude accuracy [14]. In 2022, Jingxuan Ban introduced a calibration and compensation method to mitigate temperature-induced errors in rotary optical encoders. A dedicated testing setup and a gyroscope-based calibration

approach were developed to quantify and correct these errors. Experimental validation was carried out to verify the effectiveness of the method [15].

In 2023, Ting Zhu proposed a dual-axis rotation scheme for a dual-axis rotational inertial navigation system (DRINS) to enhance reliability and positioning accuracy. By analyzing the complex error model of a DRINS and developing principles for rotation-axis switching and reciprocating rotation, an optimized rotation scheme was designed. Simulation and experimental results using a DRINS prototype demonstrated that the proposed method significantly improves navigation accuracy compared to traditional approaches [16].

Hence, this study introduces a Low-Cost single-axis rotating inertial navigation system (RINS) designed to mitigate error accumulation based on a Low-Cost IMU. After analyzing the various contributing error sources, the performance of this system is compared with that of a conventional Inertial Navigation System (INS). To enable a more precise evaluation, simulations are conducted under a defined scenario to examine the impact of errors on positioning accuracy. Finally, experimental tests were designed to validate the results, and experimental tests were conducted and compared against the simulation outcomes.

This research is organized into five sections. Section 2 presents the governing equations of the rotating inertial navigation system in detail, followed by a comprehensive analysis of the system's error sources. Section 3 outlines the conditions and parameters for the simulations, followed by a step-by-step presentation of the results. Section 4 provides an in-depth presentation of the experimental results related to the proposed system. Finally, Section 5 discusses the findings obtained from all analyses and experiments, evaluating their consistency with theoretical predictions and the developed simulation models.

2. GOVERNING EQUATIONS

The governing equations of the Inertial Navigation System are presented in Equations (1– 5) [17].

$$\dot{L} = \frac{v_n}{R_N + h} \tag{1}$$

$$\dot{\lambda} = \frac{v_e}{(R_E + h)\cos L} \tag{2}$$

$$\dot{h} = -v_d \tag{3}$$

$$[\dot{\omega}^{BN}]^B = [\omega^{BI}]^B - C_N^B([\omega^{NE}]^N + [\omega^{EI}]^N) \tag{4}$$

$$[\dot{V}_B^E]^N = [f]^N + [g_{eff}]^N - \left(2[\Omega^{EI}]^N + [\Omega^{NE}]^N\right)[V_B^E]^N \tag{5}$$

$\dot{L}$ represents the rate of change of geographic latitude, $\dot{\lambda}$ the rate of change of geographic longitude, and $\dot{h}$ the rate of change of the body's altitude above the Earth's surface. v_n, v_e and v_d denote the body velocity components toward the north, east, and down directions in the navigation frame, respectively. L is the geographic latitude, and h is the body's altitude above the Earth's surface. R_E and R_N refer to the prime-vertical radius of curvature and the meridian radius of curvature, respectively ,calculated by equations (6-7).

$$R_E = \frac{R_0}{(1 - e^2 \sin^2(L))^{0.5}} \tag{6}$$

$$R_N = \frac{R_0(1 - e^2)}{(1 - e^2 \sin^2(L))^{1.5}} \tag{7}$$

$[\omega^{BN}]^B$ denotes the angular velocity of the body frame relative to the navigation frame represented in the body frame, while $[\omega^{BI}]^B$ is the angular velocity of the body frame relative to the inertial frame expressed in the body frame. $[\omega^{NE}]^N$ represents the angular velocity of the navigation frame relative to the Earth frame, represented in the navigation frame, and $[\omega^{EI}]^N$ is the angular velocity of the Earth frame relative to the inertial frame, expressed in the navigation frame. C_N^B corresponds to the rotation matrix from the navigation frame to the body frame. $[\dot{V}_B^E]^N$ denotes the rate of change of the body velocity relative to the Earth, expressed in the navigation frame; $[f]^N$ is the specific force in the navigation frame, and $[g_{eff}]^N$ is the effective gravity in the navigation frame. Finally, $[\Omega^{EI}]^N$ and $[\Omega^{NE}]^N$ represent the skew-symmetric matrices $[\omega^{EI}]^N$ and $[\omega^{NE}]^N$, respectively.

Given that the sensor rotates at a constant angular velocity around its axis relative to the body of the vehicle, the primary difference between the rotating inertial navigation system and the conventional navigation equations is observed in Equation (8).

$$[\Omega^{BI}]^B = [\Omega^{BS}]^B + C_S^B[\Omega^{SI}]^S \quad (8)$$

It should be noted that $[\Omega^{SI}]^S$ gyroscope output and $[\Omega^{BS}]^B$ angular velocity of the body relative to the sensor, C_S^B represent the rotation matrix defining the transformation from the sensor frame to the body frame.

2.1 Error Analysis

In this section, three fundamental error sources—recognized as the primary factors contributing to divergence in system data—are analyzed and discussed. To simplify the analysis, the body frame is considered to be aligned with the navigation frame.

Gyroscope and accelerometer biases, as some of the most influential system errors, play a significant role in data divergence and are modeled in Equation (9) [6].

$$b_a = \begin{bmatrix} b_x \\ b_y \\ b_z \end{bmatrix}, \quad d_g = \begin{bmatrix} d_x \\ d_y \\ d_z \end{bmatrix} \quad (9)$$

The subscript a pertains to the accelerometer, while the subscript g corresponds to the gyroscope.

The scale factor error is considered one of the significant error sources in the system, and its modeling is presented in Equations (10 – 11).

$$S_a = \begin{bmatrix} K_{ax} & 0 & 0 \\ 0 & K_{ay} & 0 \\ 0 & 0 & K_{az} \end{bmatrix} \quad (10)$$

$$S_g = \begin{bmatrix} K_{gx} & 0 & 0 \\ 0 & K_{gy} & 0 \\ 0 & 0 & K_{gz} \end{bmatrix} \quad (11)$$

Installation error is also among the existing error sources in the system, and its modeling is provided in Equations (12 – 13).

$$N_g = \begin{bmatrix} 0 & K_{axy} & K_{axz} \\ K_{ayx} & 0 & K_{ayz} \\ K_{azx} & K_{azy} & 0 \end{bmatrix} \quad (12)$$

$$N_g = \begin{bmatrix} 0 & K_{gxy} & K_{gxz} \\ K_{gyx} & 0 & K_{gyz} \\ K_{gzx} & K_{gzy} & 0 \end{bmatrix} \quad (13)$$

Bias Error Analysis: The error equations resulting from bias, affecting the velocity of the inertial navigation system over a time interval of length T, are presented in Equations (14 – 15).

$$[b_a]^N = C_B^N C_S^B [b_a]^S \quad (14)$$

$$\int_0^T [b_a]^N dt = \begin{bmatrix} b_x T \\ b_y T \\ b_z T \end{bmatrix} \quad (15)$$

The error equations resulting from bias, affecting the attitude of the inertial navigation system over a time interval of length T, are presented in Equations (16 – 17).

$$[d_g]^N = C_B^N C_S^B [d_g]^S \quad (16)$$

$$\int_0^T [d_g]^N dt = \begin{bmatrix} d_x T \\ d_y T \\ d_z T \end{bmatrix} \quad (17)$$

To calculate the errors of the rotating inertial navigation system, the sensor coordinate frame must first be transformed to the body frame, which is accomplished using the rotation matrix presented in Equation (18).

$$C_S^B = \begin{bmatrix} \cos(\omega t) & -\sin(\omega t) & 0 \\ \sin(\omega t) & \cos(\omega t) & 0 \\ 0 & 0 & 1 \end{bmatrix} \quad (18)$$

The angular velocity of the sensor frame relative to the body frame is denoted as ω. Considering the provided rotation matrix, the bias-induced rotational error equations for the velocity of the inertial navigation system over a time interval of length T are presented in Equations (19 – 20)

$$[b_a]^N = C_B^N C_S^B [b_a]^S = \begin{bmatrix} b_x \cos(\omega t) - b_y \sin(\omega t) \\ b_x \sin(\omega t) + b_y \cos(\omega t) \\ b_z \end{bmatrix} \quad (19)$$

$$\int_0^T [b_a]^N dt = \begin{bmatrix} 0 \\ 0 \\ b_z T \end{bmatrix} \quad (20)$$

Additionally, the bias-induced error equations for the attitude of the rotating inertial navigation system over a time interval of length T are presented in Equations (21– 22).

$$[d_a]^N = C_B^N C_S^B [d_a]^S = \begin{bmatrix} d_x \cos(\omega t) - d_y \sin(\omega t) \\ d_x \sin(\omega t) + d_y \cos(\omega t) \\ d_z \end{bmatrix} \quad (21)$$

$$\int_0^T [d_a]^N dt = \begin{bmatrix} 0 \\ 0 \\ d_z T \end{bmatrix} \quad (22)$$

Scale Factor Error Analysis: The equations related to velocity errors caused by scale factor errors in the inertial navigation system over the time interval T are presented in Equations (23 – 24).

$$S_a[f]^N = C_B^N \begin{bmatrix} K_{ax} & 0 & 0 \\ 0 & K_{ay} & 0 \\ 0 & 0 & K_{az} \end{bmatrix} \begin{bmatrix} 0 \\ 0 \\ -g_{eff} \end{bmatrix} \quad (23)$$

$$\int_0^T S_a[f]^N dt = \begin{bmatrix} 0 \\ 0 \\ -g_{eff} T \end{bmatrix} \quad (24)$$

The equations related to attitude errors caused by scale factor errors in the inertial navigation system over the time interval T are presented in Equations (25 – 26).

$$S_g[f]^N = C_B^N \begin{bmatrix} K_{gx} & 0 & 0 \\ 0 & K_{gy} & 0 \\ 0 & 0 & K_{gz} \end{bmatrix} \begin{bmatrix} \Omega \cos(L) \\ 0 \\ -\Omega \sin(L) \end{bmatrix} \quad (25)$$

$$\int_0^T S_g[f]^N dt = \begin{bmatrix} K_{gx} \Omega \cos(L) \\ 0 \\ -K_{gz} \Omega \sin(L) \end{bmatrix} \quad (26)$$

Ω denotes the angular velocity of the Earth frame relative to the inertial frame, expressed in the Earth frame.

The equations related to velocity errors caused by scale factor errors in the rotating inertial navigation system over the time interval T are presented in Equations (27 – 28).

$$S_a[f]^N = C_B^N C_S^B \begin{bmatrix} K_{ax} & 0 & 0 \\ 0 & K_{ay} & 0 \\ 0 & 0 & K_{az} \end{bmatrix} \begin{bmatrix} 0 \\ 0 \\ -g_{eff} \end{bmatrix} \quad (27$$

$$\int_0^T S_a[f]^N dt = \begin{bmatrix} 0 \\ 0 \\ -g_{eff} T \end{bmatrix} \quad (28$$

The equations related to attitude errors caused by scale factor errors in the rotating inertial navigation system over the time interval T are presented in Equations (29 – 30).

$$S_g[f]^N = C_B^N C_S^B \begin{bmatrix} K_{gx} & 0 & 0 \\ 0 & K_{gy} & 0 \\ 0 & 0 & K_{gz} \end{bmatrix} \begin{bmatrix} \Omega \cos(L) \cos(\omega t) \\ -\Omega \cos(L) \sin(\omega t) \\ -\Omega \sin(L) + \omega \end{bmatrix} \quad (29$$

$$\int_0^T S_g[f]^N dt = \begin{bmatrix} \frac{\Omega \cos(L)}{2} (K_{gx} + K_{gy}) T \\ 0 \\ \left(-\Omega \sin(L) + \omega\right) K_{gz} T \end{bmatrix} \quad (30$$

Installation Error Analysis: The equations related to velocity errors caused by installation errors in the inertial navigation system over the time interval T are presented in Equations (31– 32).

$$N_a[f]^N = C_B^N \begin{bmatrix} 0 & K_{axy} & K_{axz} \\ K_{ayx} & 0 & K_{ayz} \\ K_{azx} & K_{azy} & 0 \end{bmatrix} \begin{bmatrix} 0 \\ 0 \\ -g_{eff} \end{bmatrix} \quad (31)$$

$$\int_0^T N_a[f]^N dt = \begin{bmatrix} -g_{eff} T K_{axz} \\ -g_{eff} T K_{ayz} \\ 0 \end{bmatrix} \quad (32)$$

The equations related to attitude errors caused by installation errors in the inertial navigation system over the time interval T are presented in Equations (33 – 34).

$$N_g[f]^N = C_B^N \begin{bmatrix} 0 & K_{gxy} & K_{gxz} \\ K_{gyx} & 0 & K_{gyz} \\ K_{gzx} & K_{gzy} & 0 \end{bmatrix} \begin{bmatrix} \Omega \cos(L) \\ 0 \\ -\Omega \sin(L) \end{bmatrix} \quad (33)$$

$$\int_0^T N_g[f]^N dt = \begin{bmatrix} -TK_{gxz} \Omega \sin(L) \\ TK_{gyx} \Omega \cos(L) - TK_{gyz} \Omega \sin(L) \\ TK_{gzx} \Omega \cos(L) \end{bmatrix} \quad (34)$$

The equations related to velocity errors caused by installation errors in the rotating inertial navigation system over the time interval T are presented in Equations (35 – 36).

$$N_a[f]^N = C_B^N C_S^B \begin{bmatrix} 0 & K_{axy} & K_{axz} \\ K_{ayx} & 0 & K_{ayz} \\ K_{azx} & K_{azy} & 0 \end{bmatrix} \begin{bmatrix} 0 \\ 0 \\ -g_{eff} \end{bmatrix} \quad (35)$$

$$\int_0^T N_a[f]^N dt = \begin{bmatrix} 0 \\ 0 \\ 0 \end{bmatrix} \quad (36)$$

The equations related to attitude errors caused by installation errors in the rotating inertial navigation system over the time interval T are presented in Equations (37– 38).

(37)

$$N_g[f]^N = C_B^N C_S^B \begin{bmatrix} 0 & K_{gxy} & K_{gxz} \\ K_{gyx} & 0 & K_{gyz} \\ K_{gzx} & K_{gzy} & 0 \end{bmatrix} \begin{bmatrix} \Omega\cos(L)\cos(\omega t) \\ -\Omega\cos(L)\sin(\omega t) \\ -\Omega\sin(L)+\omega \end{bmatrix}$$

(38)

$$\int_0^T N_g[f]^N dt = \begin{bmatrix} 0 \\ \frac{T\Omega\cos(L)}{2}\left(K_{gxy} - K_{gyx}\right) \\ 0 \end{bmatrix}$$

3. ERROR SIMULATIONS

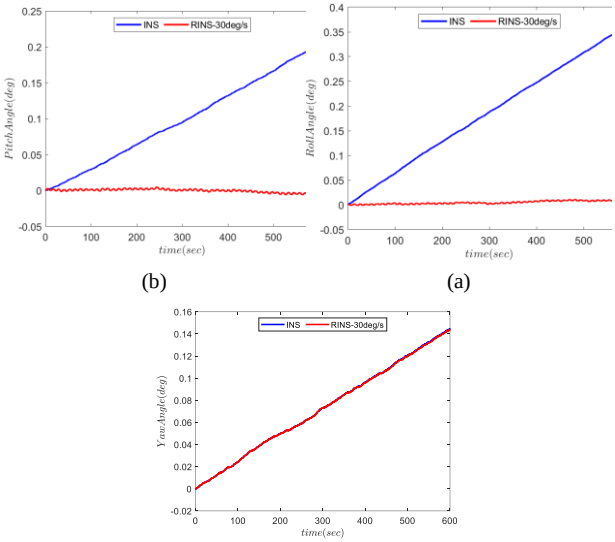
3.1 Bias Error

The simulation was performed in four stages to facilitate a detailed and distinct analysis of various error types. In the first stage, the impact of bias error was analyzed independently. Moreover, to approximate the simulated data to real-world conditions, random noise was added to the data in addition to applying structural errors. Table 1 presents the bias values of the simulated sensors.

Table 1. Simulated Values of Inertial Sensor Bias

2	X-Axis	Y-Axis	Z-Axis
Gyroscope Bias (°/h)	2	2	2
Gyroscope White Noise (°/√h)	0.2	0.2	0.2
Accelerometer Bias (m/s²)	0.002	0.002	0.002
Accelerometer White Noise (m/s/√h)	0.1	0.1	0.1

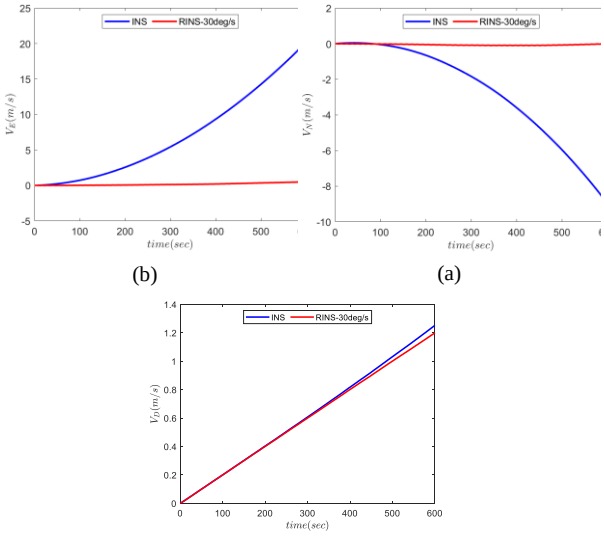
For the simulation of the rotating inertial navigation system, the sensor was set to rotate about the vertical axis (Z-axis) at an angular velocity of 30 degrees per second. As indicated by the error analysis in the previous section, when bias errors are present, the rotating inertial navigation system mitigates or eliminates errors perpendicular to the rotation axis, whereas the error along the rotation axis remains unaffected. This behavior is clearly illustrated in the graphs presented in Figures 1 and 2.



(b) (a)

(c)

Fig. 1. Bias error of the attitude during sensor rotation about the z-axis (a) Roll angle, (b) Pitch angle, (c) Yaw angle.



(b) (a)

(c)

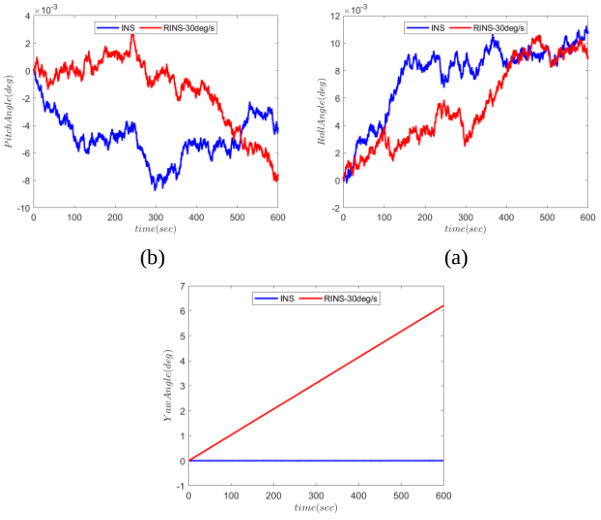
Fig. 2. Bias error of the Velocity during sensor rotation about the z-axis: (a) Velocity along North, (b) Velocity along East, (c) Velocity along Down.

3.2 Scale Factor Error

In this section, the error caused by the scale factor is examined. The scale factor values for the gyroscope and accelerometer used in the simulation are presented in Table 2. As concluded from the error analysis in the previous section, in the presence of scale factor errors, the rotating inertial navigation system tends to reduce attitude errors along the y-axis and x-axis due to the small angular velocity of the Earth's rotation, whereas the error along its rotation axis is significantly larger than that of the conventional inertial navigation system. Moreover, the velocity errors along all three axes show no significant difference between the two systems, with divergence occurring only along the rotation axis. This behavior is clearly illustrated in the graphs presented in Figures 3 and 4.

Table 2. Simulated Values of Scale Factor Errors for Inertial Sensors.

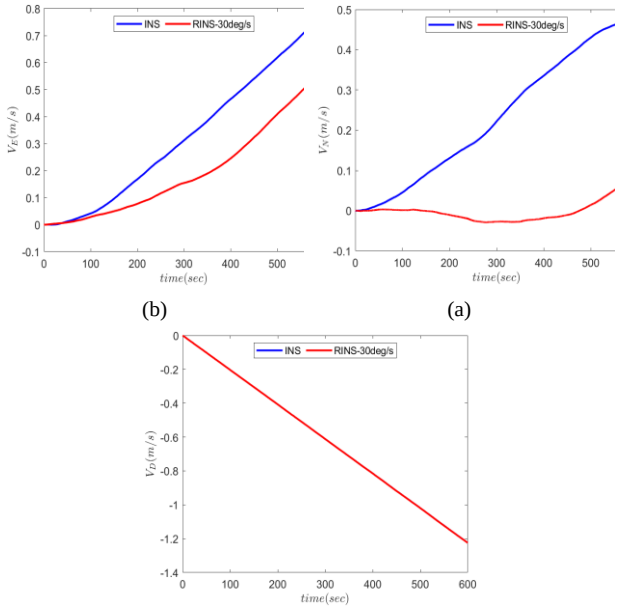
Error Type	X-Axis	Y-Axis	Z-Axis
Gyroscope Scale Factor Error (PPM)	400	400	400
Gyroscope White Noise (°/√h)	0.2	0.2	0.2
Accelerometer Scale Factor Error (PPM)	200	200	200
Accelerometer White Noise (m/s/√h)	0.1	0.1	0.1



(b) (a)

(c)

Fig. 3. Scale factor error of the attitude during sensor rotation about the z-axis: (a) Roll angle, (b) Pitch angle, (c) Yaw angle.



(b) (a)

(c)

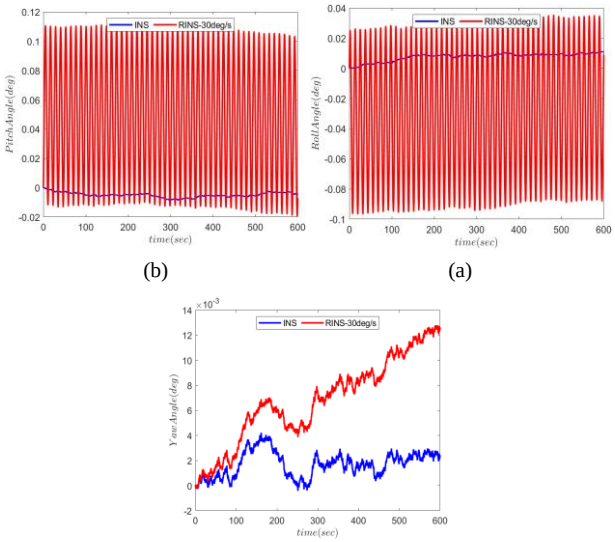
Fig. 4. Scale factor error of the Velocity during sensor rotation about the z-axis: (a) Velocity along North, (b) Velocity along East, (c) Velocity along Down.

3.3 Installation Error

In this section, the mounting error is analyzed. The values of the gyroscope and accelerometer mounting errors used are presented in Table 3. As concluded from the previous error analysis, in the presence of mounting errors, the rotating inertial navigation system tends to reduce velocity errors in directions perpendicular to the rotation axis, while the error along the rotation axis remains unchanged. Additionally, it reduces the attitude errors in all directions. This behavior is observable in the graphs shown in Figures 5 and 6.

Table 3. Simulation values of inertial sensor mounting errors.

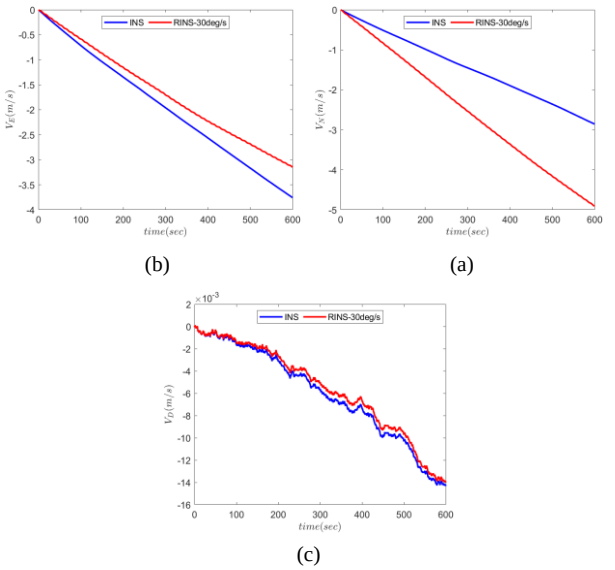
Error Type	X Axis	Y Axis	Z Axis
Gyroscope Installation Error (°)	0.04	0.04	0.04
Gyroscope White Noise (°/√h)	0.2	0.2	0.2
Accelerometer Installation Error (°)	0.04	0.04	0.04
Accelerometer white noise (m/s/√h)	0.1	0.1	0.1



(b) (a)

(c)

Fig. 5. Installation error of the attitude during sensor rotation about the z-axis: (a) Roll angle, (b) Pitch angle, (c) Yaw angle.



(b) (a)

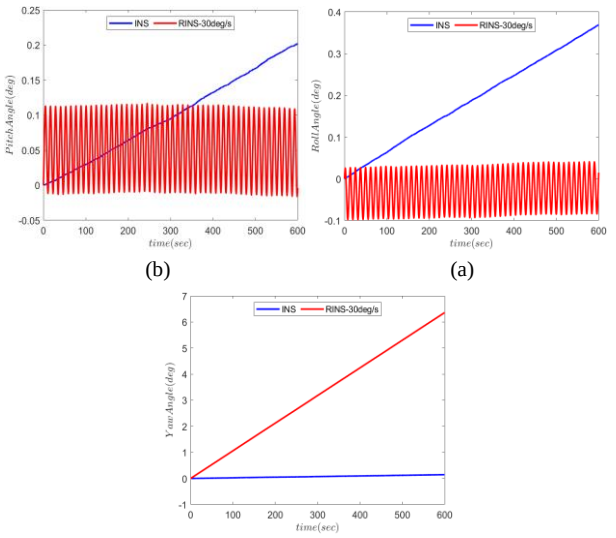
(c)

Fig. 6. Installation error of the Velocity during sensor rotation about the z-axis: (a) Velocity along North, (b) Velocity along East, (c) Velocity along Down.

3.4 Combined Error Analysis

Finally, simulations incorporating all error sources simultaneously were performed under both statistical and dynamical conditions.

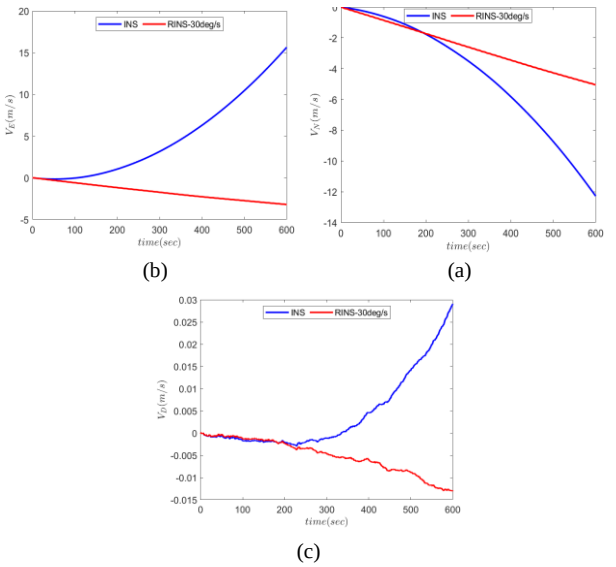
The results of the statistical simulation are presented in Figures 7 and 8. As observed from these figures, in directions perpendicular to the rotation axis, the Rotational Inertial Navigation System (RINS) demonstrates superior performance compared to the conventional inertial navigation system.



(b) (a)

(c)

Fig. 7. Combined error of the attitude during sensor rotation about the z-axis: (a) Roll angle, (b) Pitch angle, (c) Yaw angle.



(b) (a)

(c)

Fig. 8. Combined error of the Velocity during sensor rotation about the z-axis: (a) Velocity along North, (b) Velocity along East, (c) Velocity along Down.

For the dynamic simulations, a comparative analysis was conducted between rotations around the x-axis and the z-axis. As illustrated in Figures 9 and 10, the position error during rotation about the z-axis is significantly smaller than that observed in

both the conventional system and the sensor rotating about the x-axis. This demonstrates the superior stability and accuracy of the z-axis rotation configuration in maintaining positional integrity under dynamic conditions.

Furthermore, based on the results obtained from the mathematical analyses, it is evident that for the RINS operating with rotation about the x-axis, the yaw angle exhibits higher stability and improved performance compared to both the conventional RINS and the system rotating about the z-axis. This characteristic makes the x-axis configuration more suitable for applications where yaw accuracy is of primary importance.

However, considering the substantially smaller position error associated with rotation about the z-axis, this axis was selected as the preferred rotation axis for the experimental validation. Accordingly, the following sections of the paper focus on the detailed analysis and evaluation of the z-axis rotation performance.

Table 4 presents the values of the gyroscope and accelerometer mounting errors employed in the simulations, providing a clearer basis for analysis and interpretation.

Table 4. Simulation values of inertial sensor mounting errors.

Error Type	X Axis	Y Axis	Z Axis
Gyroscope Bias (°/h)	-9	13	-8
Accelerometer Bias (m/s²)	0.0088	-0.0127	0.0078
Gyroscope Scale Factor Error (PPM)	$S_g = \begin{bmatrix} 400 & -300 & 250 \\ 0 & -300 & -150 \\ 0 & 0 & -350 \end{bmatrix} ppm$		
Gyroscope White Noise (°/√h)	2.91×10^{-6}		
Accelerometer Scale Factor Error (PPM)	$S_a = \begin{bmatrix} 500 & -300 & 200 \\ -150 & -600 & 250 \\ -250 & 100 & 450 \end{bmatrix} ppm$		
Accelerometer White Noise (m/s/√h)	0.000981		

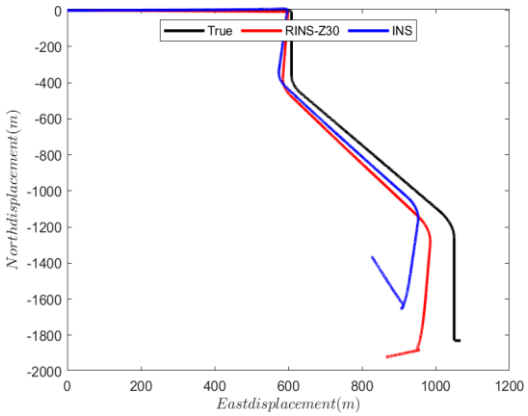


Fig. 9. North and East displacement errors during sensor rotation about the z-axis.

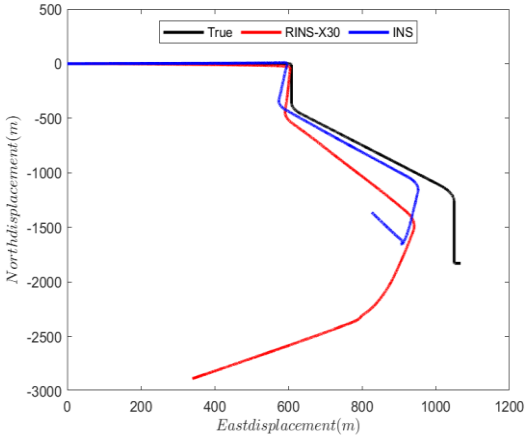


Fig. 10. North and East displacement errors during sensor rotation about the x-axis.

4. EXPERIMENTAL TEST

In this section, the simulation is experimentally validated to assess the accuracy of the proposed model. For this purpose, the sensor is mounted on a table as shown in Figure 11 and rotated clockwise about the z-axis at a speed of 65 degrees per second. As observed from the results presented in Figures 12 and 13, the rotating inertial navigation sensor effectively reduces errors in directions perpendicular to its axis of rotation. At the same time, it is noted that the sensor only increases the error along the rotation axis, indicating certain limitations in its performance in this direction. These experimental findings are in full agreement with the simulation results discussed in the previous section, confirming the validity and precision of the simulations. But it is expected that the attitude and velocity components perpendicular to the rotational

axis do not perfectly match the simulation results. This discrepancy arises primarily from the rotational rate error of approximately ±0.05°/s in the turntable and the misalignment of the rotational axis. Moreover, since the turntable does not provide encoder data for precise angular rate measurement, a constant angular rate was assumed in the INS computation. These factors collectively contribute to the observed differences between the simulation and experimental results.

However, despite the existing errors in the experimental test, the rotational inertial navigation system performed better than the conventional inertial navigation system. Moreover, by improving the laboratory equipment, even better results can be achieved from this system.

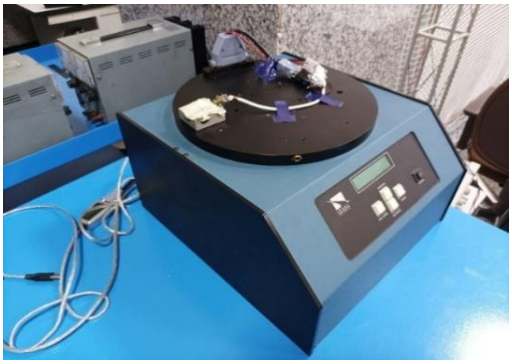


Fig. 5. Experimental Setup.

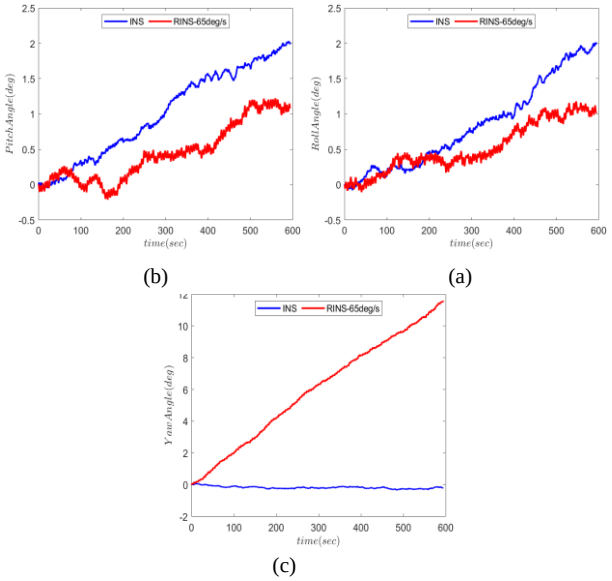


Fig. 11. Experimental Test error of the attitude during sensor rotation about the z-axis: (a) Roll angle, (b) Pitch angle, (c) Yaw angle.

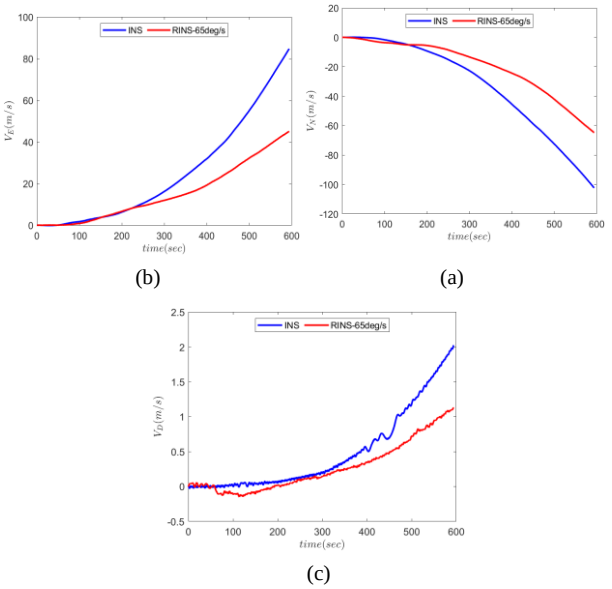


Fig. 12. Experimental Test error of the Velocity during sensor rotation about the z-axis: (a) Velocity along North, (b) Velocity along East, (c) Velocity along Down.

5. CONCLUSION

In this study, a comparison was made between the performance of the Rotary Inertial Navigation System and the traditional Inertial Navigation System. For a more precise evaluation, a theoretical analysis of the errors in both systems was first presented, followed by a simulation-based examination and comparison of the related sensors' performance. Subsequently, to validate the simulation results, experimental tests were designed and conducted to assess the accuracy of the rotary inertial navigation system under real-world conditions. Although the experimental results are expected to closely match the simulation outcomes, noticeable discrepancies remain. These deviations primarily result from the rotational rate error (approximately ±0.05°/s) of the turntable, misalignment of the rotational axis, and the assumption of a constant angular rate during INS computation. Despite these factors, the results confirm that the Rotary Inertial Navigation System (RINS) effectively reduces navigation errors, except along the axis of rotation.

Acknowledge: This research was supported by the Vice Presidency for Research of Sharif University of Technology, and the authors gratefully acknowledge the financial support provided under Grant No. G4030414.

CONFLICT OF INTERESTS

No conflict of interest has been expressed by the authors.

REFERENCES

[1] P. Groves, *Book Principles of GNSS, Inertial and Multi-Sensor Integrated Navigation Systems*, 2nd ed. London, Artech House, 2013.

[2] C. Jekeli, *Inertial Navigation Systems with Geodetic Applications.* Berlin, New York, Walter de Gruyrer, 2001.

[3] C. L. Glennie, K. P. Schwarz, A. M. Forsberg, A. V. Olesen, and K. Keller, "A comparison of stable platform and strapdown airborne gravity," *Journal of Geodesy*, vol. 74, no. 5, pp. 383-389, 2000, https://doi.org/10.1007/s001900000082.

[4] D. Titterton and J. Weston, *Strapdown Inertial Navigation Technology*. 2nd ed. IET, 2004.

[5] K. R. Britting, *Inertial Navigation Systems Analysis*. New York, Wiley-Interscience, 1971.

[6] G. Arthur, *Applied Optimal Estimation*. MIT press, 1974.

[7] Y. Y. Ben, Y. L, Chai, W. Gao, and F. Sun, "Analysis of error for a rotating strap-down inertial navigation system with fibro gyro," *Journal of Marine Science and Application*, vol. 9, no. 4, pp. 419-424, 2010, https://doi.org/10.1007/s11804-010-1028-z.

[8] E. S. Geller, "Inertial system platform rotation," *IEEE Transactions on Aerospace and Electronic Systems*, vol. aes-4, pp. 557-568, 1968, https://doi.org/10.1109/TAES.1968.5409024.

[9] C. S. Giovanni and E. Levinson, "Performance of a ring laser strapdown Marine Gyrocompass," *Navigation*, vol. 28, no. 4, pp. 311-341, 1981, https://doi.org/10.1002/j.2161-4296.1981.tb00779.x.

[10] Y. Yong and L. J. Miao, "Fiber-optic strapdown inertial system with sensing cluster continuous rotation," *IEEE Transactions on Aerospace and Electronic* Systems, vol. 40, no. 4, pp. 1173-1178, 2004, https://doi.org/10.1109/TAES.2004.1386872.

[11] L. D. Zhang, J. X. Lian, M. P. Wu, and Z. q. Zheng, "Research on auto compensation technique of strap-down inertial navigation systems," in *International Asia Conference on Informatics in Control, Automation and Robotics*, Bangkok, Thailand, 2009, https://doi.org/10.1109/CAR.2009.80.

[12] S. Du, "Rotary inertial navigation system with a low-cost MEMS IMU and its integration with GNSS," Ph.D. dissertation, University of Calgary, Calgary, Canada, 2015, https://doi.org/10.11575/PRISM/27695.

[13] S. Tianxiao, K. Li, l. Wang. J. Sui, and L. Wang, "A rapid and high-precision initial alignment scheme for dual-axis rotational inertial navigation system," *Microsystem Technologies*, vol. 23, no. 12, pp. 5515-5525, 2017, https://doi.org/10.1007/s00542-017-3286-z.

[14] Z. Liu, L. Wang, K. Li, and H. Han, "Analysis and improvement of attitude output accuracy in tri-axis rotational inertial navigation system," *IEEE Sensors Journal*, vol. 20, no. 11, pp. 6091-6100, 2020, https://doi.org/10.1109/JSEN.2020.2972557.

[15] J. Ban, G. chen, l. Wang, and Y. meng, "A calibration method for rotary optical encoder temperature error in a rotational inertial navigation system," *Measurement Science and Technology*, vol. 33, no. 6, 2022, Art. no. 065203, https://doi.org/10.1088/1361-6501/ac4c67.

[16] T. Zhu, L. Wang, T. Zou, and G. Peng, "A dual-axis rotation scheme for redundant rotational inertial navigation system," *Micromachines*, vol. 14, no. 2, 2023, Art. no. 351, https://doi.org/10.3390/mi14020351.

[17] P. H. Zipfel, *Modeling And Simulation of Aerospace Vehicle Dynamics*. American Institute of Aeronautics and Astronautics, Inc. 2000.